Black holes, redshift and quasars

COLIN ROURKE
ROSEMBERG TOALA ENRIQUEZ
ROBERT S MACKAY

We outline a model for quasar radiation. The model is based on the simplest black hole accretion model. It allows for significant gravitational redshift, fitting (currently discredited) observations of Arp et al, and provides a natural explanation for the apparently paradoxical phenomena uncovered by Hawkins; it also provides a plausible explanation for the low emissions of Sagittarius A^*. In order for this model to be plausible, a mechanism for absorbing angular momentum needs to be given. For this we rely on the observation made in [22] that inertial drag allows a black hole to absorb angular momentum.

83C57

Models for black holes (BHs) and their radiation are central to modern astrophysics. For an overview, see Meier [14].

The purpose of this paper is to investigate a simple model whose significance appears to have been overlooked in the literature. This model is spherically symmetric, fully relativistic and based on the Schwarzschild metric. Gravitational redshift plays an important part in the theory, and this probably explains observations of Sgr A^*, whose luminosity is several orders of magnitude below the Eddington limit – a fact which is hard to explain with existing models. The point here is that the received radiation is redshifted due to the gravitational field of the BH and, if the redshift is $1+z$, then the received luminosity is multiplied by the factor $(1+z)^{-2}$ which, for suitable parameter values, may be several orders of magnitude below unity. Thus Sgr A^* may well be radiating at approximately the Eddington limit but because of this effect does not appear to be doing so. (For details here, see the end of Section 7.)

The model is intended to provide an explanation for high observed quasar redshift consistent with the (currently discredited) observations of Arp et al [3, 6], and it suggests a simple model for observed quasar variability, which in turn provides an explanation for the apparently paradoxical phenomena uncovered by Hawkins [8]. We do not expect that this simple model will be the final model that will be adopted for quasars. Rather, our aim is merely to demonstrate, by example, that there are plausible models for

quasars with significant gravitational redshift, and therefore the reasons used historically to decide that all redshift in quasars is cosmological were spurious.

One important point needs to be made at the outset. One of the principal reasons for discarding the gravitational theory for redshift concerns angular momentum. If the surrounding medium for the black hole has even a very small angular momentum about the centre, then conservation of angular momentum will create large tangential velocities as infalling matter approaches the centre and this will tend to choke off the inflow and prevent accretion. This has lead to the subject being dominated by the theory of accretion discs. If the observed radiation comes from an accretion disc affected by local gravitational effects, there would be wide spectral lines (redshift gradient) and not narrow ones as observed.

However it is a simple consequence of the inertial drag effects discussed in [18], a rotating body can absorb angular momentum (see for example the solution in [19, Equation (7) page 7] with $C = 0$ which has angular momentum per unit mass zero for $r = 0$ and growing like r for r big).

If angular momentum can be nullified by central rotation, then it does not force the existence of an accretion disc and redshift can be largely gravitational. Moreover there is a feedback effect working in favour of this. If the incoming matter has excess angular momentum, then it will tend to contribute to the central rotation which therefore changes to increase the inertial drag effect until the two balance again. Conversely, if there is a shortfall, the black hole will slow down. In other words, once locked on the ambient conditions that allow the black hole to accrete, there is a mechanism for maintaining that state. For more detail here see [20, Section 6] and [22].

The conclusion is that we can effectively ignore the angular momentum obstruction for accretion and this is what we will do in this paper.

In our model, black holes radiate by converting the gravitational energy of incoming matter into radiation. There are two significant regions: an optically thin outer region and an optically thick inner regions which are separated by a sphere which we call the Eddington sphere. The radiation that we see comes from a narrow band near the Eddington sphere and which is all at roughly the same distance from the central black hole. This allows the radiation to exhibit a consistent redshift. One of the main arguments for discarding the gravitational theory for quasar redshift is that proximity to a large mass causes “redshift gradient”. If redshift is due to a local mass affecting the region where radiation is generated, then the gravitational gradient from approach to the mass would spread out the redshift and result in very wide emission lines. But in

our model, because the observed radiation comes only from near the Eddington sphere, there is no redshift gradient.

There are fully relativistic Schwarzschild BH solutions to be found in the literature, for example the models of Flammang, Thorne and Zytkow [5] quoted by Meier (ibid, page 490). But the significance of these models, and in particular their redshift, appears to have been overlooked, perhaps because of the angular momentum problem discussed earlier.

The basic set-up that we shall consider is a BH floating in gas of Hydrogen atoms (the *medium*), which might be partially ionised (ie form a plasma), with the radiation coming from accretion energy. Matter falls into the BH and is accelerated. Interaction of particles near the BH changes the "kinetic energy" (KE) of the incoming particles into thermal energy of the medium and increases the degree of ionisation. The thermal energy is partially radiant and causes the perceived BH radiation.

Kinetic energy is not a relativistic concept as it depends on a particular choice of inertial frame in which to measure it. It is for this reason that we have placed it in inverted commas. Nevertheless, it is a very useful intuitive concept for understanding the process being described here.

The following simple considerations suggest that most of the KE of the infalling matter is converted into heat and available to be radiated outwards. A typical particle is very unlikely to have purely radial velocity. A small tangential velocity corresponds to a specific angular momentum. As the particle approaches the BH, conservation of angular momentum causes the tangential velocity to increase. Thus the KE increase due to gravitational acceleration goes largely into energy of tangential motion. Different particles are likely to have different directions of tangential motion and the resulting melée of particles all moving on roughly tangential orbits with varying directions is the main vehicle for interchange of KE into heat and hence radiation. Very little energy remains in the radial motion, to be absorbed by the BH as particles finally fall into it. Thus the overall radial motion of particles is slow. In terms of the models of [5] we are using the "breeze solutions" for radial flow [14, Figure 12.2, page 489]. Far away from the BH, where density is close to ambient density, and therefore low, this process converts angular momentum into radial motion with little loss of energy and serves to allow the plasma to settle into the inner regions, where the density is higher and the particle interactions generate heat and radiation.

1 Overview of the model

For simplicity of exposition we shall now assume that the medium is a Hydrogen plasma and the heavy particles are therefore protons. This is true in the higher temperature parts of the model, for example once we reach the Eddington sphere, see below. But there is no material difference if the medium is in fact a partially ionised Hydrogen gas.

Observations of quasars often show the presence of other atomic material in the radiation zone so that this simplifying assumption may need revision at a later stage.

There are three important spheres.

The outermost sphere is the Bondi sphere of radius B defined by equating the root mean square velocity $\sqrt{3kT/m_H}$ of protons in the medium with the escape velocity $\sqrt{2GM/B}$. Here T is the temperature of the medium at the Bondi radius, M is the mass of the BH, G is the gravitational constant, k is Boltzmann's constant and m_H is the mass of a proton. Thus:

$$B = \frac{2GMm_H}{3kT} \tag{1}$$

Note that we have used the Newtonian formula for escape velocity, which, as we shall recall later, is also correct in Schwarzschild geometry.

The significance of the Bondi sphere is that protons in the medium are trapped (on average) inside this sphere because they have KE too small to escape the gravitational field of the BH. The mass of matter per unit time trapped in this way is called the *accretion rate* A and can be calculated as

$$A = 2B^2 n\sqrt{2\pi kTm_H} \tag{2}$$

where n is the density of the medium (number of protons per unit volume).

Here are the details for this calculation. Maxwell's distribution for the radial velocity v_r has density $\sqrt{m_H/2\pi kT}e^{-m_Hv^2/2kT}$, so the mean $\bar{v}_r$ over inward velocities is

$$\int_0^\infty 2\sqrt{\frac{m_H}{2\pi kT}}e^{-m_Hv^2/2kT}v\,dv\,.$$

Put $u = m_Hv^2/2kT$ to obtain

$$\int_0^\infty 2\sqrt{\frac{kT}{2\pi m_H}}e^{-u}\,du = 2\sqrt{\frac{kT}{2\pi m_H}}.$$

Then $A = 4\pi B^2 nm_H\bar{v}_r/2 = 2B^2 n\sqrt{2\pi kTm_H}$.

Proceeding inwards, the next important sphere is the Eddington sphere of radius R which is defined by equating outward radiation pressure on the protons in the medium with inward gravitational attraction from the BH. More precisely, the outward radiation pressure acts on the electrons in the medium which in turn pull the protons by electrical forces. This is the same consideration as used to define the Eddington limit for stars and this is why we have used the same name. At the Eddington sphere the gravitational pull on an incoming proton is balanced by the outwards radiation pressure (mediated by electrons) and, assuming the radiation pressure is just a little bigger, the acceleration of the incoming proton is replaced by deceleration and the KE of infall is absorbed by the medium and available to feed the radiation. It is a definite hypothesis that there is an Eddington sphere, but, we shall see that the final model that we construct using this hypothesis does fit facts pretty well, and this justifies it.

It is helpful to think of the Eddington sphere as a transition barrier akin to the photosphere of a star. Indeed the Eddington radius R is also the radius at which photons get trapped in the medium and for this reason is also known as the trapping radius. This can be seen by thinking of the forces that define it the other way round. The incoming matter flow exerts a force on the outward radiation and when these two are in balance, the outward radiation is stopped and photons are trapped.

Thus at the Eddington sphere we have two things happening: the infalling protons are stopped and their KE released into the general pool of thermal energy and the outward flow of radiation is also stopped. Thus radiation from the BH is generated by activity in the close neighbourhood of the Eddington sphere and this is the place where redshift of the outward radiation due to the gravitational pull of the BH arises.

We shall give precise formulae that allow us to determine the Eddington radius in terms of the other parameters in Section 3.

The final sphere is the familiar Schwarzschild sphere or event horizon of radius $S = 2GM/c^2$ where M is the BH mass.

We shall call the region between the Schwarzschild and Eddington spheres the *active region* and the region between the Bondi sphere and the Eddington sphere, the *outer region*. We shall make a simplifying assumption that nearly all the KE that powers the BH is released in the active region. This means that we are ignoring any KE turned into heat by particle interaction in the outer region. This is justified by the fact that this region has low density, close to the ambient density, so that most particle interactions are between particles sufficiently far apart to conserve kinetic energy. It is useful to think of this region as a "settling region" where angular momentum is converted into

radial motion, allowing the plasma to settle towards the active region. See also the discussion below equation (6) and in Section 8.

We shall also make one other simplifying assumption: we shall assume that there is no significant increase in temperature near the Bondi sphere due to the BH radiation. Ie T is the ambient temperature.

2 Previous work on quasars and gravitational redshift

Before starting work on the details of the energy production it is worth reviewing the historical reasons for abandoning the idea that quasars might have significant instrinsic (gravitational) redshift and why they do not apply to our model. There are four main reasons why redshift in quasars has traditionally not been believed to be intrinsic.

(1) Redshift gradient (see the discussion in [17] on pages 3–4)

If redshift is due to a local mass affecting the region where radiation is generated, then the gravitational gradient from approach to the mass would spread out the redshift and result in very wide emission lines. This effect is called "redshift gradient".

In our model, although the energy production takes place throughout the active region, the emitted radiation is generated only at (or near) the Eddington sphere which is all at the same distance from the central mass and subject to the same redshift. Thus our model has the observed property that emission lines are moderately narrow.

(2) Forbidden lines (cf Greenstein–Schmidt [7])

Many examples of BH radiation show so-called forbidden lines, which can only be produced by gas or plasma at a fairly low density. The assumption that *all* the radiation is produced by a low density region leads to an implausibly large and heavy mass (see [7, page 1, para 2]).

In our model, the region directly adjacent to the Eddington sphere is at roughly ambient density which is, in all examples that we have examined, low enough to support forbidden lines (more details on this will be given in Section 6). A narrow shell of low density near the Eddington sphere is excited by the radiation produced at the sphere and produces radiation in turn. It is here that forbidden transitions take place and result in the observed forbidden lines.

(3) Mass and variability problems (cf Greenstein–Schmidt [7], Hoyle–Fowler [10])

The mass problem is a rider on the forbidden line problem but also applies to attempts at models for gravitational redshift without significant redshift gradient. As remarked above, assuming that all the radiation is produced by a low density region leads to an implausibly large and heavy mass. The same thing happens if one tries to produce a region with sufficient local gravitational field to provide a base for the radiation production, without redshift gradient, as for example in Hoyle and Fowler [10]. This problem is compounded by the fact that quasars typically vary with time scales from days to years. For variability over a short timescale, a small production region is needed (significantly smaller than the distance that light travels in one period).

It is worth remarking in passing that this problem is unresolved by the current assumption that all quasar redshift is cosmological. This implies that quasars are huge and very distant so that special (and to our mind unnatural) mechanisms are invoked to explain variability.

In our model, the size of the radiation producing region is small enough. The BH sizes that we find fitting observations are in the range 10^3 to 10^8 solar masses. For quasars with significant intrinsic redshift, the radius of the Eddington sphere has the same order of magnitude as the Schwarzschild radius, and for 10^8 solar masses this is 3×10^{11} metres or 10^3 light seconds or about 20 light minutes. Thus the natural mechanism for variability, namely orbiting clouds or more solid bodies causing periodic changes in observed luminosity, fits the facts perfectly.

It is also worth observing here that there is a quite remarkable paper of M R S Hawkins [8], which proves an apparently paradoxical result, namely that a certain sample of quasars exhibits redshift without time dilation. The paradox arises from the fact that redshift and time dilation are identical in general relativity. Indeed they are identical in any theory based on space-time geometry. What Hawkins actually finds is a sample of quasars with varying redshift for which the macroscopic variation in light intensity does not correlate with the redshift. The resolution of the paradox is that the mechanism that produces the redshift and the mechanism which causes the variability are not subject to the same gravitational field. This is precisely how our model works. The redshift is caused by the central BH and the variability is caused by orbiting clouds etc, much further out, and in a region of lower redshift. For more detail on the Hawkins paper and its meaning see [21]. Properly understood, the paper proves conclusively that quasars typically have intrinsic redshift.

(4) Statistical surveys

Stockton [23] is widely cited as a proof that quasar redshift is cosmological. He takes a carefully selected sample of quasars and searches for nearby galaxies within a small angular distance and at close redshift. Out of a chosen sample of 27 quasars, he finds a total of 8 which have nearby galaxies with close redshifts. He assumes that all these quasars have significant intrinsic redshifts and are therefore not actually near their associated galaxies. He then calculates the probability of one of these coincidences occurring by chance at about 1/30, and concludes that the probability of this number of coincidences all occurring by chance is about 1.5 in a million.

The conclusion he draws is that all quasar redshift is cosmological.

The fallacy is obvious from this summary. It may well be that many of the quasars in the survey do not have significant intrinsic redshift and therefore some of these coincidences are not chance events. The model that we provide in this paper allows for the gravitational redshift of a quasar to vary from near zero to as large as you please. In the next section we shall find a formula for redshift in terms of the central mass and the parameters of the medium (density and temperature). Roughly speaking, redshift is small (orders of magnitude smaller than 1) if the mass is big or the medium is dense and cold. Conversely, with a small mass and a hot thin medium, the redshift can be several orders of magnitude greater than 1. We shall have more to say about this in the final section of the paper, but there is a natural progression for a quasar, as it accretes mass and grows heavier, to start with a very high gravitational redshift and gradually evolve towards a very low one. Without a sensible population model for quasars, it is difficult to comment on the number of coincidences that Stockton finds, but it is highly plausible that heavy quasars (with low gravitational redshift and central masses of say 10^7 to 10^9 solar masses) gravitate towards galactic clusters and therefore have nearby galaxies at a similar cosmological redshift. This would provide a natural framework for the Stockton survey within our model.

Stockton does discuss the possibility that quasars may have both small and large intrinsic redshifts (see [23, page 753, right]), but the discussion is marred by assuming that the two classes must be unrelated objects. Our model has a natural progression between the two classes.

There is a more modern survey by Tang and Zhang [24] which also claims to prove that all quasar redshift is cosmological. But examining the paper carefully, what is actually proved is that some particular models for quasar birth and subsequent movement are incompatible with observations. To comment properly on this paper we would again need a good population model for quasars. But it is worth briefly mentioning that at

least one of their models (ejection at 8×10^7 m/s from active galaxies with a lifespan of 10^8 years) does fit facts fairly well, see [24, figure 1, page 5]. The ejection velocity is implausibly large, but the lifespan could easily be 50 times larger allowing for a plausible ejection velocity of say 10^7 m/s and a better fit with the data.

Finally, there is another interesting argument given by Wright [26] "proving" that quasar redshift is all cosmological from details of the spectra. This is the Lyman-alpha-forest argument. These observations he cites give useful information about the outer region and we shall return to this near the end of the paper in Section 8.

3 Kinetic energy, escape velocity and redshift

We now start on the detailed calculations of the energy production.

Throughout the paper we use the standard Schwarzschild metric

$$c^2\,ds^2 = -Q\,c^2\,dt^2 + \frac{1}{Q}\,dr^2 + r^2\,d\Omega^2, \tag{3}$$

where $Q = 1 - S/r = 1 - 2GM/c^2r$. Here t is thought of as time, r as radius and $d\Omega^2$, the standard metric on the 2–sphere, is an abbreviation for $d\theta^2 + \sin^2\theta\,d\phi^2$ (or more symmetrically, for $\sum_{j=1}^3 dz_j^2$ restricted to $\sum_{j=1}^3 z_j^2 = 1$). Note that $\sqrt{-ds^2}$ can be regarded as proper time.

We start by discussing KE. As remarked earlier, this is not a relativistic concept. It makes sense in Minkowski space where there is the Einstein formula for the KE of a particle of mass m moving with velocity v

$$mc^2\left(\frac{1}{\sqrt{1 - v^2/c^2}} - 1\right) \tag{4}$$

and therefore it makes sense in an inertial frame of reference.

Consider a particle falling freely and radially into a Schwarzschild BH (and hence following a geodesic). Use τ for proper time along this geodesic. Let $\dot{r}$ denote $dr/d\tau$. The MacKay–Rourke paper [15] describes two natural flat observer fields, the escape field and the dual capture field. We use the latter. This gives a foliation by geodesics following inward freefall paths with orthogonal flat space slices (ie isometric to Euclidean 3–spaces). Thus we have local coordinates with time being proper time along the geodesics and space defined by flat Euclidean coordinates in the orthogonal space slices. These local coordinates provide convenient inertial frames in which to measure KE.

Now the flat slices are derived by making the distance between spheres of area $4\pi r_1^2$ and $4\pi r_2^2$ be $|r_2 - r_1|$ and hence r is a Euclidean coordinate and it follows that $\dot{r}$ is the correct definition of radial velocity for calculating KE. For tangential velocity, θ, ϕ provide standard spherical coordinates in this inertial frame and the usual Euclidean formula for velocity in (r, θ, ϕ) (again measured wrt τ) provides the correct velocity v to measure KE in equation (4).

We also need a formula for escape velocity. MacKay and Rourke provide this in [15, Equation (10)] namely $\dot{r} = c\sqrt{1-Q} = \sqrt{2GM/r}$. [MacKay and Rourke use natural units with $G = c = 1$, we have added a factor c to convert to MKS units.]

In the next section we shall derive these formulae by a simple direct analysis but first we give the promised formula from which the Eddington radius can be read.

Recall the standard equation for the luminosity at the Eddington limit, [14, page 5]

$$L_E = \frac{4\pi}{\kappa} GMc \tag{5}$$

where κ is the radiative opacity for electron scattering which is usually taken to be $0.4\text{cm}^2/\text{g}$ or 4×10^{-2} in MKS units [14, page 5]. The Eddington radius R is defined by the same considerations and hence this gives the radiation from the Eddington sphere. Note that this formula does not depend on the radius of the radiating sphere. Since it corresponds to local balance of forces, it is true in a relativistic setting provided we state exactly where we are applying it. We are applying it near the Eddington sphere.

Now assume that the luminosity is, within a factor X, the same as the KE of accreted matter falling onto the Eddington sphere. The intuitive description that we gave earlier of the nature of the Eddington sphere suggests that about $1/2$ of the KE released on "impact" should be radiated outwards and about $1/2$ absorbed into the medium below so that X is roughly $1/2$. But, as we shall see later, there is also energy arriving upwards from inside the sphere, and this suggests a larger figure for X. We shall return to this estimate later, but for now keep X as a parameter to be determined.

Equating X times the KE released on impact with the Eddington luminosity we find

$$X A c^2 \left(\frac{1}{\sqrt{1 - v^2/c^2}} - 1 \right) = \frac{4\pi}{\kappa} GMc \tag{6}$$

where $v = 2GM/R$ is the escape velocity at R, the velocity of freely infalling matter. Matter does not in fact arrive radially because of tangential motion, which is amplified by conservation of angular momentum as described earlier. However the energy of motion available to be absorbed and re-radiated is unaffected by the transfer of energy

from radial to partially tangential and therefore there is no error in assuming that motion is radial here.

It is worth digressing a little here. A particle in the outer region with significant tangential velocity may not reach the Eddington sphere. This happens if the tangential velocity, amplified by conservation of angular momentum, absorbs all the KE and the radial velocity slows to zero. But, because of the mechanics near the Bondi sphere described earlier, particles cannot escape the outer region in significant numbers. We are assuming implicitly that we have a steady state on timescales short compared with that given by the accretion rate. It follows that excess tangential velocity in the outer region must be transmuted into radial velocity by non-thermal particle interaction as suggested earlier. Thus in this region particle interaction allows the plasma to "settle" inwards towards the Eddington sphere, without significant loss of KE. This settling process will need to be modelled in detail in a further paper. At this stage we just assume that it takes place. There are some features of the process that can be deduced from observations and we shall discuss this further in Section 8.

It is not hard to solve equation (6) to find an explicit formula for the Eddington radius R in terms of the other parameters. For calculation purposes however, it is far more convenient to use redshift which has a simple relationship to R. For a Schwarzschild BH, redshift $1+z$ at a radius with escape velocity v is $1/\sqrt{1-v^2/c^2} = 1/\sqrt{1-S/R}$, since $v = 2GM/R$, and hence $1 - S/R = (1+z)^{-2}$ or

$$S = R(1-(1+z)^{-2}). \tag{7}$$

But in terms of z, equation (6) gives the following simple formula for the observed redshift for a BH radiating from the Eddington sphere:

$$z = \frac{4\pi MG}{Ac\kappa X} \tag{8}$$

and then substituting for A and B we have:

$$z = \frac{4\pi MG}{2(\frac{2GMm_H}{3kT})^2 n\sqrt{2\pi kTm_H}\, c\kappa X}$$

and collecting terms:

$$z = 2^{-1}\, 9\sqrt{\pi/2}\, \kappa^{-1}\, M^{-1}\, n^{-1}\, (kT)^{1.5}\, m_{\mathrm{H}}^{-2.5}\, G^{-1}\, c^{-1}\, X^{-1} \tag{9}$$

4 Potential and kinetic energy in Schwarzschild space-time

In this section we give the promised direct calculation using Schwarzschild geometry for the formulae used in Section 3 for KE and escape velocity.

We will take the approach that a particle is fundamentally described by its 4–momentum, that is, by $P = mU$, where $m = \sqrt{-\langle P, P\rangle}$ is the rest mass of the particle and $U = (\dot{t}, \dot{r}, \dot{\theta}, \dot{\phi})$ is its 4–velocity and dot represents differentiation with respect to proper time.

Consider a particle falling freely in Schwarzschild spacetime, that is following a geodesic path. There are conserved quantities associated to the symmetries of the Schwarzschild spacetime. Here we focus on

$$E_0 = -\langle P, \partial_t \rangle.$$

It is tempting to interpret E_0 as the energy measured by a static observer, however this is misleading since ∂_t does not have unit-length and hence does not correspond to a physical observer. There is one exception though, at infinity ∂_t corresponds to an observer comoving with the gravitational source, so we are led to interpret E_0 as the energy of the particle measured at infinity by a static observer.

Correspondingly, we regard

$$E := -\langle P, \frac{1}{\sqrt{Q}}\partial_t \rangle = \frac{E_0}{\sqrt{Q}},$$

as the energy measured by an *interior* static observer, where $Q = 1 - \frac{2GM}{c^2 r}$. Explicitly we have, $E = \dot{t}E_0\sqrt{Q}$.

As the particle falls inwards it gains potential energy

$$\text{PE} := E_0 - E = E_0 \left(1 - \frac{1}{\sqrt{Q}}\right)$$

and the relativistic expression for the Kinetic energy can be written as the difference between the observed energy and the rest energy of the particle,

$$\text{KE} := E - mc^2$$

and we obtain a conservation law of the form

$$\text{KE} + \text{PE} = E_0 - mc^2$$

where the RHS can be interpreted as the kinetic energy available at infinity. For example, it vanishes when the particle is falling at escape velocity, cf equation (12).

Now we elaborate on the formula for KE. The proper time parametrisation condition translates to

$$\langle P, P\rangle = -m^2$$

which, for a particle falling radially, reduces to

$$-Qc^2\dot{t}^2 + Q^{-1}\dot{r}^2 = -c^2 \tag{10}$$

This in turn can be written as a single ODE for r, using the conservation of "energy",

$$\dot{r}^2 = c^2\left(\frac{E_0^2}{m^2c^4} - Q\right). \tag{11}$$

From this we can deduce the escape velocity as measured by proper time. Note that for the particle to get asymptotically to infinity ($\dot{r} = 0$ at $r = \infty$) we need $mc^2 = E_0$. Hence the velocity necessary to achieve this is

$$\dot{r}_{\text{escape}} = \pm c\sqrt{1-Q} = \pm\sqrt{\frac{2GM}{r}}, \tag{12}$$

so we recover the classical value.

Remark These geodesics, namely the ones that follow $(\dot{t},\dot{r}) = (\frac{1}{Q}, \pm c\sqrt{1-Q})$, are precisely the natural observer fields found by MacKay and Rourke and they correspond to a stream of test particles falling at precisely at escape velocity.

Returning to kinetic energy, note that

$$\begin{aligned}\text{KE} &= mc^2\left(\frac{E}{mc^2} - 1\right)\\ &= mc^2\left(\frac{\dot{t}E_0\sqrt{Q}}{mc^2} - 1\right).\end{aligned}$$

Dividing (10) by $\dot{t}^2$ we get

$$\dot{t} = \sqrt{\frac{Q}{Q^2 - u^2/c^2}},$$

where $u = \frac{\dot{r}}{\dot{t}}$ is the velocity measured by the static coordinates. However, it will be convenient to use the velocity measured by the MacKay–Rourke natural flat observers, that is

$$v = \frac{dr}{d\tau} = \frac{dr}{dt}\frac{dt}{d\tau} = \frac{u}{Q}$$

Therefore the kinetic energy can be written as:

$$\text{KE} = mc^2\left(\frac{E_0}{mc^2\sqrt{1-v^2/c^2}} - 1\right)$$

Note that for the case of a particle falling at escape velocity this reduces to:

$$\text{KE} = mc^2\left(\frac{1}{\sqrt{1-v^2/c^2}} - 1\right)$$

5 The critical radius and high redshift BHs

Before inserting numbers to compare with observations, there are a couple more pieces of theory. Consider a particle infalling from ouside the BH and suppose that at radius r it releases all its KE, which radiates outwards. The KE is $\mathrm{KE}(r) = mc^2(1/\sqrt{Q} - 1)$ where $Q = 1 - 2GM/rc^2 = 1 - v^2/c^2$ and $v = \sqrt{2GM/r}$ the escape velocity at r. The energy $E(r)$ received outside the BH is $Q = 1/(1+z)^2$ times this in other words

$$E(r) = mc^2(\sqrt{Q} - Q) \tag{13}$$

which is ≥ 0 and zero when $v = 0$ and when $v = c$. The first is natural and obvious but the second is counterintuitive. KE $\to \infty$ as the particle approaches the speed of light at the Schwarzschild radius and you expect the released energy to $\to \infty$ as well. It doesn't.

This mistake occurs in the literature in several places. See for example the discussion in the introduction to [4]. There is no observational difference between a BH and a super-dense neutron star whose surface is just a little bit above the event horizon. The error is to ignore the redshift reduction in radiated energy.

$E(r)$ has a simple maximum when $Q = 1/4$ so there is a maximum energy released. This depends *only on m and not on M*. Again highly counterintuitive. What does depend on M is the *critical radius* $r = 4S/3$ at which this maximum is achieved. Here $1 - v^2/c^2 = 1/4$ or $v = c\sqrt{3}/2$ and $E(r) = mc^2/4$.

Inside the critical radius the received energy drops off sharply and this allows us to obtain a bound on the radiated energy for BHs whose Eddington radius is $\leq 4S/3$ or equivalently with redshift (calculated at the Eddington sphere) $1 + z \geq 2$ or $z \geq 1$. Let's call these BHs *high redshift BHs*.

The KE for an infalling particle $P(r) = \mathrm{KE}(r) = mc^2(1/\sqrt{Q} - 1)$ represents the maximum energy available to be converted into radiation at that radius, see Section 4. We can think of this conversion as analogous to friction. The medium inside the Eddington radius is "sticky" and slows the particle down, releasing energy. Now let's normalise so that all radiated energy is measured as received outside the BH. This means we multiply by $1/(1+z)^2 = Q$. Assume that the emissions come from inside the critical radius so that the received energy per unit r–distance is decreasing monotonically. Once a portion of $P(r)$ is converted to radiation, it is not replaced, so for maximum effect it needs to be radiated outwards as soon as possible. In other words the maximum possible radiation outwards is obtained by keeping the inward velocity as low as possible (very small KE). So for a bound we assume all the KE available at the Eddington radius is

radiated outwards and within the Eddington radius we can set $\dot{r} = 0$ and we get the upper bound for the extra energy received outside the BH from below the Eddington radius R:

$$\begin{aligned} -mc^2 \int_S^R Q \frac{dQ^{-\frac{1}{2}}}{dr} dr \\ = mc^2 \int_S^R Q \frac{Q^{-\frac{3}{2}}}{2} \frac{dQ}{dr} dr \\ = mc^2 [\sqrt{Q}] \text{ evaluated at } R \end{aligned}$$

Since $Q \leq (1/2)\sqrt{Q}$ in this range, this is within a factor 2 of the KE arriving at the Eddington radius from above, and hence the total possible energy radiated outwards is 3 times this KE. In other words, in terms of the notation of Section 3, we have proved $X \leq 3$. However, the assumption that all this energy radiates outwards is unrealistic and the earlier estimate of $X = 1/2$ is much more reasonable.

Note The same analysis gives a rough upper bound for BHs with small redshift but the result $\sqrt{Q}$ evaluated at the Eddington radius may be far larger than the Eddington luminosity and not provide a useful upper bound. Indeed as $r \to \infty$ it tends to mc^2.

6 Calculations

We now compare our model numerically with observations. In this section we shall calculate various parameters and, in the next section, test their fit with data. We use MKS units throughout, work to 3 sf, and use the following constant values:

$\kappa = 4 \times 10^{-2}$, $k = 1.38 \times 10^{-23}$, $m_{\mathrm{H}} = 1.67 \times 10^{-27}$, $G = 6.67 \times 10^{-11}$, $c = 3 \times 10^{8}$.

Redshift in terms of medium factor and mass

The key equation is the redshift equation (9):

$$z = 2^{-1}\, 9\sqrt{\pi/2}\, \kappa^{-1}\, M^{-1}\, n^{-1}\, (kT)^{1.5}\, m_{\mathrm{H}}^{-2.5}\, G^{-1}\, c^{-1}\, X^{-1}$$

For convenience (and familiarity) we express M in solar masses; in other words we write $M = \mathcal{M}\, M_{\mathrm{sun}} = 2 \times 10^{30}\, \mathcal{M}$, where $\mathcal{M}$ is the BH mass in solar masses. Substituting for κ, k, m_H, G, c we find the numerical version:

$$z = 1.27 \times 10^{7}\, \mathcal{M}^{-1}\, n^{-1}\, T^{1.5}\, [1/(2X)] \tag{14}$$

For simplicity we shall use the default value ($\frac{1}{2}$) for X which is the same as ignoring the expression in square brackets. If further information on X comes to light, we can reinstate it.

The factor $n^{-1}\,T^{1.5}$ depends only the ambient medium; we will call it the *ambient coefficient* and use the notation Θ. Recall that n is the density in particles (protons) per cubic metre and T is the ambient temperature in degrees Kelvin.

The equation now takes the simple form:

$$z = 1.27 \times 10^7 \,\frac{\Theta}{\mathcal{M}} \tag{15}$$

To get an idea of the range of possible values for Θ, interstellar density is estimated at between 10^2 and 10^{12} where the thinner regions are associated with higher temperatures, which vary inversely with the density from about 10^5 to 10 [1]. Thus Θ varies from about $10^{5.5}$ at the high end (hot thin plasma) to $10^{-10.5}$ at the low end (cold dense gas). [An aside here: "dense" is a relative term. The density of the atmosphere is 10^{25}, and the interstellar density is always far smaller then a laboratory "high vacuum" of about 10^{16}.]

As you can see immediately, the redshift depends critically on the nature of the ambient medium, which can cause it to vary by 16 orders of magnitude. By contrast, the variation with mass, which might be in the range 10^4 to 10^8 solar masses, is far smaller, a further 4 orders of magnitude. For example, suppose we have a BH of mass $10^7\,M_{\text{sun}}$ (a little bigger than Sgr A*), so that $10^7\,\mathcal{M}^{-1} = 1$, then avoiding the extremes for the ambient coefficient, the redshift might vary from 10^{-7}, in other words so small that there is no measurable redshift, up to 10^3 which is so big that the redshift reduction factor in received luminosity, $(1+z)^{-2}$ or about 10^{-6}, makes it extremely unlikely that we could detect the quasar unless, like Sgr A*, it is very close to us.

Two remarks at this point:

(1) We promised to comment on the maximum density that supports the observed forbidden lines. This is estimated by Greenstein and Schmidt to be about 3×10^{10} [7, third paragraph of abstract] which fits nearly all the densities that we have been considering, missing just the extreme cold, dense media.

(2) It is worth looking at the data for Sgr A* since it has just been mentioned. This has mass $4.6 \times 10^6\,M_{\text{sun}}$ and according to our model should have redshift varying from about 10^{-10} to 10^6. A redshift of 10^4 would imply that the received luminosity was 10^{-8} of the Eddington limit, which is exactly what is observed [4, page 1357 top right]. Thus our model suggests that the lack of luminosity for Sgr A* is due to a rather hot,

thin medium near this BH. We will return to examine the data for Sgr A* in detail, at the end of Section 7.

Three types of redshift and the Hubble formula

The redshift $z = z_{\text{grav}}$ used by the model (and quantified above) is the *gravitational* aka *intrinsic* redshift. But when you observe a quasar, you see the *observed* redshift z_{obs} which depends on both the gravitational redshift z_{grav} and the cosmological redshift z_{cos} which is a function of distance.

The relationship between the three is

$$1 + z_{\text{obs}} = (1 + z_{\text{grav}})(1 + z_{\text{cos}})$$

which, provided at least one of z_{grav} or z_{cos} is fairly small, can conveniently be approximated as:

$$z_{\text{obs}} \approx z_{\text{grav}} + z_{\text{cos}}$$

From the cosmological redshift you can read the distance d by the Hubble formula $d = cz_{\text{cos}}/H$ where H is the Hubble constant $2.2 \times 10^{-18}\text{sec}^{-1}$. Substituting for c we have:

$$d = 1.35 \times 10^{26}\, z_{\text{cos}} \tag{16}$$

The other observed datum is magnitude which we will discuss below. From the magnitude and the distance you can calculate the mass. But you need the cosmological redshift, which is not observed, to find the distance. Deciding how to split the observed redshift into intrinsic and cosmological is not simple. The best we can do is to try various splits and see how they fit. There are however examples (which we shall call *Arp* quasars) where the observations suggest a galaxy at the same distance as the quasar so that we can use the redshift for this galaxy for z_{cos}.

We shall look at specific examples of both these in the next section.

Luminosity and magnitude

The main observed data for a quasar are redshift and luminosity, which has a simple relationship to magnitude:

$$L_{\text{obs}} = 2.87 \times 10^{-8} \times 10^{-\frac{2}{5}\text{mag}}$$

This is the received luminosity in W/m^2 and the calculation is based on comparison with the solar luminosity ($1.3kw/m^2$) and magnitude (-26.7). In our model, the emitted luminosity is always the Eddington luminosity which depends purely on the BH mass:

$$L_E = \frac{4\pi}{\kappa} GMc = 1.26 \times 10^{31} \mathcal{M} \tag{17}$$

From this you can calculate the received luminosity by applying three correction factors. The first two are straightforward. Use the inverse square law and divide by $1/4\pi$ to convert from total emitted luminosity to received luminosity per unit area and secondly apply redshift correction $(1 + z_{\text{obs}})^{-2}$. (If redshifts are small, this second factor can be ignored.)

The third factor is more problematic. Magnitude is usually measured using visible wavelengths, but BH radiation covers a far wider spectrum. This implies that the observed magnitude underestimates the luminosity by a factor of perhaps 10 or larger. Further the radiation from the BH is attenuated by intervening clouds for which there is strong evidence (see the discussion in Section 8) and this gives a further underestimate, which is again difficult to quantify but which might also be up to a factor of 10. Let's call the result of these two the *magnitude correction factor*, denoted Φ, and note that it might vary between 1 and 100 or more.

Thus we have

$$L_{\text{obs}} = \frac{L_E}{4\pi\,\Phi\, d^2 (1 + z_{\text{obs}})^2}$$

and substituting for the luminosities and distance (using equation (16)), we get the following formula for mass in terms of magnitude and redshifts:

$$\mathcal{M} = \frac{2.87}{1.26} 10^{-31} \times 4\pi\,\Phi \times (1.35)^2 \times 10^{52} \times z_{\cos}^2 (1 + z_{\text{obs}})^2 \times 10^{-8} \times 10^{-\frac{2}{5}\text{mag}}$$

which simplifies to:

$$\mathcal{M} = \Phi \times 5.22 \times 10^{(14 - \frac{2}{5}\text{mag})} \times z_{\cos}^2 (1 + z_{\text{obs}})^2$$

To get a feeling for this formula, we shall anticipate the first example in the next section where the data are treated more accurately. Objects 2 and 3 in NGC7603 (see Figure 1) both have mag ≈ 20 and $z_{\cos} \approx .03$ (taken from the main galaxy) so the formula gives approximately:

$$\mathcal{M} = \Phi \times 5 \times 10^3$$

The gravitational redshift is approx .3 and substituting for $\mathcal{M}$ in the redshift formula (15) gives:

$$\Phi \approx 10^4 \Theta$$

Thus with $\Phi = 1$ (no magnitude correction) we have a black hole of mass about 5×10^3 solar masses floating in a medium of ambient coefficient 10^{-4} which is pretty cold and dense medium. Perhaps the visible filament in which these objects appear to be immersed is a cold dense cloud. Or perhaps, the magnitude correction should be about 100 and the mass 5×10^5, which seems a more likely mass for a quasar, with the medium having a less extreme ambient coefficient of about 10^{-2}.

We finish this section with formulae for the Eddington radius and the temperature of the Eddington sphere (assuming the radiation is black body).

Eddington radius

We have $1 - S/R = (1+z)^{-2}$ where S is Schwarzschild radius and R is Eddington radius. Write $\zeta = S/R = 1 - (1+z)^{-2}$ and notice that for small z, $\zeta = 2z + O(z^2)$. Since the Schwarzschild radius of the sun is 3×10^3 m we have:

$$R = 3 \times 10^3 \, \mathcal{M}/\zeta \tag{18}$$

Radiant temperature

Suppose the radiation is effectively black body with temperature T_B (notation intended to keep distinct from T which is ambient temperature used earlier). Stefan-Boltzmann gives total luminosity $4\pi R^2 \sigma T_B^4$, where $\sigma = 5.67 \times 10^{-8}$ and equating this with Eddington luminosity we have:

$$4\pi \times 9 \times 10^6 \, \mathcal{M}^2 \times 5.67 \times 10^{-8} \, T_B^4/\zeta^2 = 1.26 \times 10^{31} \, \mathcal{M}$$

which gives:

$$T_B^4 = 1.96 \times 10^{30} \, \mathcal{M}^{-1} \, \zeta^2 \tag{19}$$

Example $\mathcal{M} = 10^6$, $z = .1$ so that $\zeta^2 \approx .04$ then $T_B \approx 1.67 \times 10^5$.

7 Data

We now proceed to examples, that is, given the data $z_{\cos}$, z_{grav} and magnitude we use the model to deduce luminosity, mass, ratio R/S, distance to Earth and temperature of the source as if it were a black body.

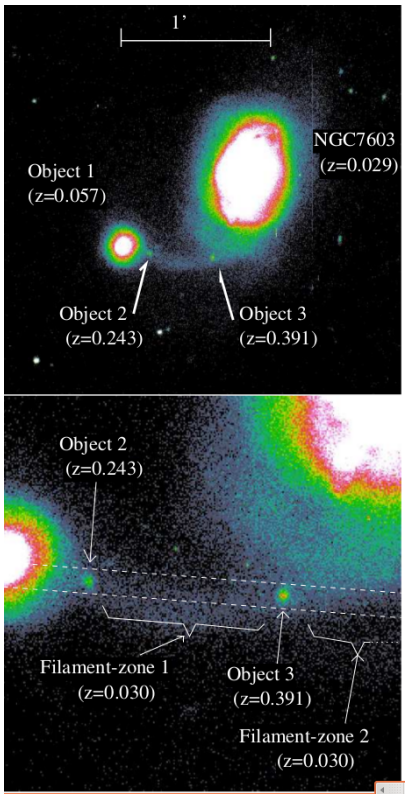

Figure 1: NGC 7603 and the surrounding field. R-filter, taken on the 2.5 m Nordic Optical Telescope (La Palma, Spain). Reproduction of Figure 1 of [13]

We shall continue to use the default value $\frac{1}{2}$ for X and ignore the correction factor Φ (ie assume that it is 1). To take these into account, use the following rules. Multiply Θ by $X/2$ and further multiply both $\mathcal{M}$ and Θ by Φ.

First we consider the system around NGC 7603, previewed in the last section, which appears to contain two Arp quasars (objects 2 and 3 in Figure 1). Lopez Corredoira and Gutierrez [13] report $z = 0.0295$ and $B = 14.04$ mag for the main galaxy, NGC 7603. A fact that attracted attention is its proximity to NGC 7603B (Object 1 hereafter), a spiral galaxy with higher redshift $z = 0.0569$, moreover a filament can be observed connecting both galaxies. They also found two objects superimposed on the filament with redshifts 0.394 ± 0.002 and 0.245 ± 0.002 for the objects closest to and farthest from NGC 7603, Objects 3 and 2, respectively. B–magnitudes corrected for extinction (due to the filament) are respectively 21.1 ± 1.1 and 22.1 ± 1.1 [13].

They go on to say "If we consider the redshifts as indicators of distance, the respective absolute magnitudes would be : $M_V = -21.5 \pm 0.8$ and -18.9 ± 0.8. However, if we consider an anomalous intrinsic redshift case (in such a case, in order to derive the distance, we set $z = 0.03$), the results are: $M_V = -15.2 \pm 0.8$ and -13.9 ± 0.8 resp. In this second case, they would be on the faint tail of the HII-galaxies, type II; they would be dwarf galaxies, 'tidal dwarfs', and this would explain the observed strong star formation ratio: objects with low luminosity have higher EW(H_α). Of course, this would imply that we have non-cosmological redshifts. . . . From several absorption lines we estimated the redshift of the filament apparently connecting NGC 7603 and NGC 7603B as $z = 0.030$, very similar to the redshift of NGC 7603 and probably associated with this galaxy."

From this analysis we are led to set $z_{\cos} = 0.03$ for the group and $z_{\text{grav}} = z - z_{\cos}$. Hence the Hubble distance, $d = c \times z_{\cos}/H = 13.5 \times 10^{25} \times z_{\cos}$, is 4.05×10^{24} metres in this case.

Next, the ratio between the Eddington radius and the Schwarzschild radius is $R/S = 1/1 - (1 + z_{\text{grav}})^{-2}$, this gives 18.6, 3.12 and 2.17 for Objects 1, 2 and 3, where we have taken z_{grav} equal to 0.028, 0.213 and 0.361, respectively.

The luminosity (in W/m^2 received at Earth) is given in terms of the magnitude by $L_{\text{mag}} = 2.87 \times 10^{-8} \times 10^{-\frac{2}{5}mag}$. We obtain 5.468×10^{-15}, 5.468×10^{-17} and 7.904×10^{-17} for Objects 1, 2 and 3, respectively.

We obtain the mass by comparing the formulae for the Eddington luminosity and the magnitude luminosity, $\mathcal{M} = M/M_{\text{sun}} = 4\pi d^2 L_{\text{mag}} \times (1+z)^2 \times 1.26^{-1} \times 10^{-31}$. We find $\mathcal{M} = 9.45 \times 10^4$, 1.32×10^3 and 2.39×10^3 for objects 1, 2 and 3, respectively.

The temperature of the quasar as if it were a black body is given by Stefan's law $T_B = \left(L(1+z)^2/\sigma 4\pi R^2\right)^{\frac{1}{4}}$ and in terms of previous data it is

$$T_B = \left(L_{\text{mag}}(1+z)^2 \times 1/\sigma \times d^2 \times \left(S/R\right)^2 \times \left(1/\mathcal{M}\right)^2 \times \left(1/S_{\text{sun}}\right)^2\right)^{\frac{1}{4}}.$$

For Objects 1, 2 and 3 we get 4.95×10^5, 3.52×10^6 and 3.63×10^6, respectively.

Finally, the ambient coefficient is defined by $\Theta = 10^{-7}\, z\, \mathcal{M}$, which helps to constraint the possible values of the ambient density and temperature. For the case at hand we get 2.07×10^{-4}, 2.19×10^{-5} and 6.75×10^{-5} for objects 1, 2 and 3, resp.

We have written a spreadsheet for these calculations, and the results for these and several more examples, are in the tables which follow. Included are two quasars (3C273 and 3C48) for which we do not know the redshift split and for which we have tried various splits. The examples come from Galianni, Arp, Burbidge, etal [6], Lopez Corredoira and Gutierrez [12, 13], Greenstein and Schmidt [7], and Hoyle and Burbidge [9].

Lopez Corredoira-Gutierrez

	INPUTS				OUTPUTS							
		z		Magnitude	R/S	L_{mag}	Solar masses	Distance	T_B	T_B * 1/1+z		Ambient coefficient
	Obs	Cos	Grav			W/m^2					X	$n^{-1} * T^{1.5}$
NGC 7603	0.029	0.03	0	14.04	-	6.948E-14	1.136E6	4.050E24	-	-	-	-
Object 1	0.058	0.03	0.028	16.8	1.861E1	5.469E-15	9.449E4	4.050E24	4.951E5	4.816E5	0.5	2.067E-4
Object 2	0.243	0.03	0.213	21.8	3.121E0	5.469E-17	1.316E3	4.050E24	3.519E6	2.901E6	0.5	2.189E-5
Object 3	0.391	0.03	0.361	21.4	2.173E0	7.905E-17	2.394E3	4.050E24	3.631E6	2.668E6	0.5	6.752E-5
NEQ 3												
Object 1	0.1935	0.12	0.0735	19.8	7.562E0	3.450E-16	1.040E5	1.620E25	7.582E5	7.063E5	0.5	5.973E-4
Object 2	0.1939	0.12	0.0739	19.6	7.525E0	4.148E-16	1.252E5	1.620E25	7.257E5	6.758E5	0.5	7.226E-4
Object 3	0.2229	0.12	0.1029	20.2	5.621E0	2.387E-16	7.596E4	1.620E25	9.513E5	8.625E5	0.5	6.107E-4
Object 4	0.1239	0.12	0.0039	17.3	1.290E2	3.450E-15	9.097E5	1.620E25	1.068E5	1.064E5	0.5	2.772E-4
GC 0248+430	0.051	-	-	-	-	-	-	-	-	-		-
QSO 1	1.311	0.051	1.26	17.45	1.243E0	3.005E-15	7.253E5	6.885E24	1.151E6	5.091E5	0.5	7.140E-2
QSO 2	1.531	0.051	1.48	21.55	1.194E0	6.885E-17	2.001E4	6.885E24	2.881E6	1.162E6	1.5	6.940E-3
B2 1637+29	0.086	-	-	-	-	-	-	-	-	-		-
Partner	0.104	0.086	0.018	-	-	-	-	-	-	-		-
Aligned QSO	0.568	0.086	0.482	20	1.836E0	2.870E-16	8.470E4	1.161E25	1.620E6	1.093E6	1.5	9.568E-3

Hoyle-Burbidge, Arp-Burbidge-et al

	INPUTS				OUTPUTS							
		z		Magnitude	R/S	L_{mag}	Solar masses	Distance	T_B	T_B * 1/1+z		Ambient coefficient
	Obs	Cos	Grav			W/m^2					X	$n^{-1} * T^{1.5}$
NGC 4319	0.0057	0.0057	0	-	-	-	-	7.695E23	-	-		-
MK 205	0.07	0.0057	0.0643	14.5	8.534E0	4.549E-14	3.041E4	7.695E23	9.706E5	9.120E5	0.5	1.528E-4
NGC 3067	0.0047	0.0047	0	-	-	-	-	6.345E23	-	-		-
3C 232	0.533	0.0047	0.5283	15.8	1.749E0	1.374E-14	1.288E4	6.345E23	2.658E6	1.739E6	0.5	5.314E-4
ESO 1327-2041	0.018	0.018	0	-	-	-	-	2.430E24	-	-		-
QSO 1327-206	1.17	0.018	1.152	16.5	1.275E0	7.209E-15	1.965E5	2.430E24	1.575E6	7.318E5	0.5	1.769E-2
Gal 0248+430	0.051	0.051	0	-	-	-	-	6.885E24	-	-		-
Q 0248 +430	1.1311	0.051	1.0801	17.45	1.301E0	3.005E-15	6.144E5	6.885E24	1.173E6	5.638E5	0.5	5.185E-2
Gal Abell 2854	0.12	0.12	0	-	-	-	-	1.620E25	-	-		-
2319+272 (4C 27.50)	1.253	0.12	1.133	18.6	1.282E0	1.042E-15	1.240E6	1.620E25	9.911E5	4.646E5	0.5	1.098E-1
NGC 3079	0.00375	0.00375	0	-	-	-	-	5.063E23	-	-		-
0958+559	1.17	0.00375	1.16625	18.4	1.271E0	1.253E-15	1.502E3	5.063E23	5.336E6	2.463E6	0.5	1.368E-4
Arp, Burbidge, et al.												
NGC 7319	0.022	0.022	0	-	-	-	-	2.970E24	-	-		-
QSO	2.114	0.022	2.092	21.79	1.117E0	5.519E-17	4.640E3	2.970E24	4.293E6	1.388E6	0.5	7.583E-4

Greenstein-Schmidt

	INPUTS				OUTPUTS								
		z		Magnitude	R/S	L_{mag}	Solar masses	Distance	T_B	T_B * 1/1+z		Ambient coefficient	Spectral index
	Obs	Cos	Grav			W/m^2					X	$n^{-1} * T^{1.5}$	
3C 273	0.1581	0.001	0.1571	12.6	3.951E0	2.617E-13	4.768E3	1.350E23	2.437E6	2.106E6	0.5	5.852E-5	0.9
	0.1581	0.01	0.1481	12.6	4.143E0	2.617E-13	4.768E5	1.350E24	7.496E5	6.529E5	0.5	5.517E-3	0.9
	0.1581	0.05	0.1081	12.6	5.388E0	2.617E-13	1.192E7	6.750E24	2.888E5	2.606E5	0.5	1.007E-1	0.9
	0.1581	0.1	0.0581	12.6	9.363E0	2.617E-13	4.768E7	1.350E25	1.514E5	1.431E5	0.5	2.164E-1	0.9
	0.1581	0.158	1E-04	12.6	5.001E3	2.617E-13	1.190E8	2.133E25	5.066E3	5.066E3	0.5	9.299E-4	0.9
3C 48	0.3675	0.001	0.3665	16.2	2.153E0	9.503E-15	3.224E2	1.350E23	6.022E6	4.407E6	0.5	9.231E-6	1.25
	0.3675	0.01	0.3575	16.2	2.187E0	9.503E-15	3.182E4	1.350E24	1.896E6	1.397E6	0.5	8.886E-4	0.95
	0.3675	0.05	0.3175	16.2	2.359E0	9.503E-15	7.492E5	6.750E24	8.286E5	6.290E5	0.5	1.858E-2	0.95
	0.3675	0.1	0.2675	16.2	2.649E0	9.503E-15	2.774E6	1.350E25	5.638E5	4.448E5	0.5	5.797E-2	0.95
	0.3675	0.2	0.1675	16.2	3.754E0	9.503E-15	9.413E6	2.700E25	3.489E5	2.988E5	0.5	1.232E-1	0.95
	0.3675	0.367	0.0005	16.2	1.001E3	9.503E-15	2.328E7	4.955E25	1.704E4	1.703E4	0.5	9.093E-4	0.95

Finally we consider data for Sgr A*. According to [4], the received luminosity is $1.85 \times 10^{-13}\ W/m^2$ which is approximately 10^{-8} of the Eddington limit. Accordingly we set $z_{\text{grav}} = 10^{-4}$ and we have the following data in the same format as above.

Sgr A* data

z			R/S	L_{mag}	Solar masses	Distance	T_B	T_B * 1/1+z		Ambient coefficient
Obs	Cos	Grav		W/m^2	$\mathcal{M}$				X	$n^{-1} * T^{1.5}$
10^4	0	10^4	100	1.185E-13	4.500E6	2.592E20	5.269E5	5.268E1	0.5	3.516E3

This table predicts the observed temperature for Sgr A* of about 50 K, which fits well with observations in the radio frequency range. The spectrum of Sgr A* from Narayan–McClintock [16, page 6] is reproduced in Figure 2.

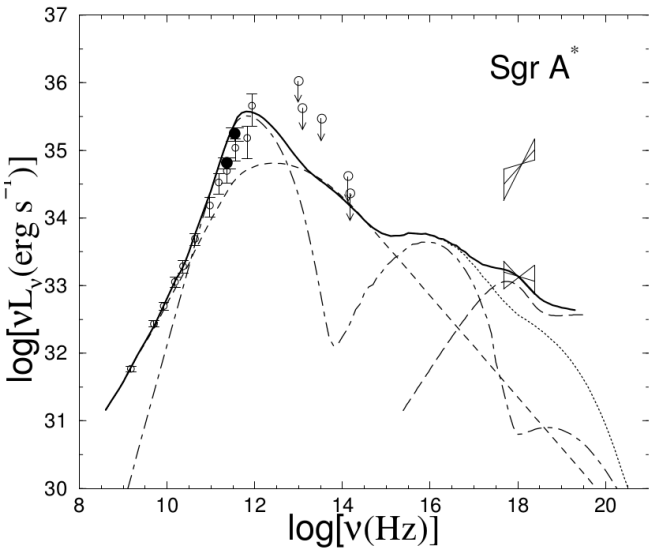

Figure 2: Figure 3 from [16] where the following references can be found. The radio data are from Falcke et al (1998; open circles) and Zhao et al (2003; filled circles), the IR data are from Serabyn et al (1997) and Hornstein et al. (2002), and the two "bow-ties" in the X-ray band correspond to the quiescent (lower) and flaring (higher) data from Baganoff et al (2001, 2003).

Ignoring the solid and dotted lines (which are attempts to fit the data with current models), the radio frequency observations and infra-red observations (up to about 10^{14} Hz) are a pretty good fit for a black body radiator with peak output at about 5×10^{12} Hz which corresponds to a temperature of about 50 K (see the frequency-dependent formulation of Wien's law in [2]) and fits our data well. Note that the actual temperature of the Eddington sphere is 5×10^5 K; it is the apparent temperature, after redshift adjustment, which is 50 K. The extreme redshift of Sgr A* explains why the principal radiation falls in the radio frequency range. The two "bow-ties" are probably due to activity remote from the actual BH, perhaps associated with orbiting clouds in the outer

region. This illustrates clearly that our model is merely a first approximation to reality, applying only to the main BH radiator, and omits other important features.

8 Conclusions

In this paper we have investigated a very simple model for BH radiation which appears to explain the observations of Arp and the paper of Hawkins [8], both of which suggest that quasars typically exhibit redshift that is not cosmological.

It is not suggested that the model is a perfect fit for all the facts. One obvious set of data that need a more complicated model are the Spectral Energy Distributions (SEDs) for quasars which are typically quite complicated and far from simple black body graphs; for a fairly simple example see Figure 3 right. By contrast, the composite spectrum on the left does have the rough outline of a black body, suggesting that the basic mechanism

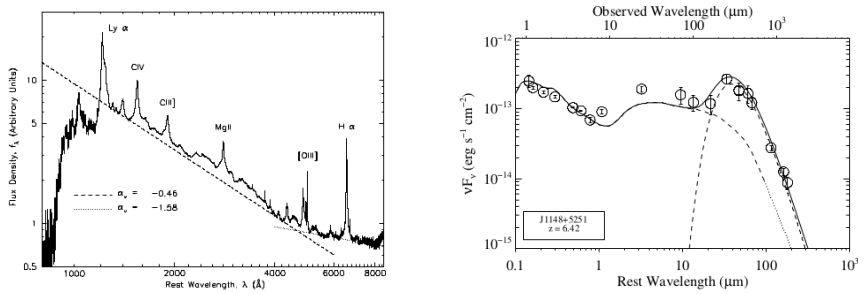

Figure 3: Left: composite spectrum (figure 3 from [25]) Right: spectrum of the $z = 6.42$ quasar SDSS J1148+5251 (figure 1 from [11])

for radiation is by thermal excitation, as in our model. One obvious suggestion for correcting SEDs is to take into account the orbiting clouds, responsible for the observed variation in radiation and which absorb radiation. The spectrum on the right could plausibly result from a black body spectrum which is partially obscured causing the two dips at the top. Or perhaps, like Sgr A* there is a black body radiator in the longer wavelengths with some short wavelength activity from the outer region superimposed.

Another strong piece of evidence (apart from variability) for the existence of orbiting clouds is the so-called "Lyman-alpha-forest". The clouds on the path to us cause absorption lines and the principal line is the L_α–line. The clouds are all at different redshifts and these lines form a forest, see Figure 4. The existence of the L_α–forest is used by Wright [26] to prove (fallaciously) that Arp is wrong about intrinsic redshift.

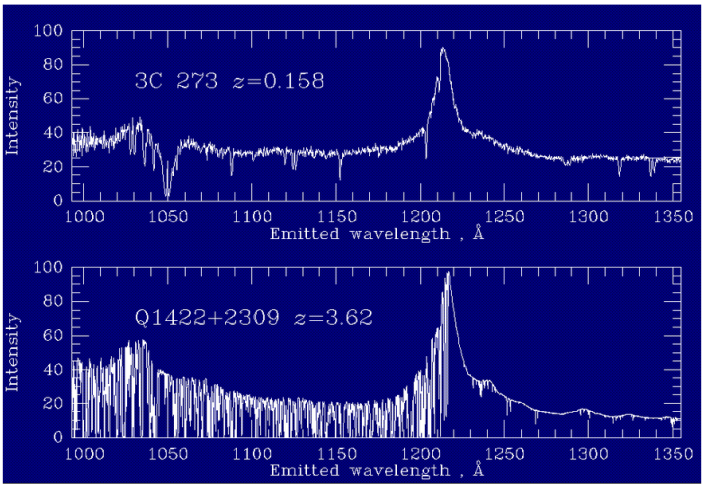

Figure 4: The Lyman Alpha Forest at low and high redshift, taken from [26]

He assumes that if the redshift is intrinsic then it jumps down suddenly away from the quasar and therefore there should be a gap to the left of the main L_α emission line before the forest starts. But the absorption clouds can orbit as close as they like to the Eddington sphere, and there is no reason for there to be a gap.

The L_α–forest suggests strongly that the settling process, that we have hypothesised taking place in the outer region, tends to form strata. This is plausible because once a stratum of greater density starts to build up, then interaction with other particles becomes more likely, and this will often result in material added to the stratum. This is analogous to the instability observed in many queuing or draining situations (for example traffic congestion with most of the traffic locked up in stationary bands at any one time). These strata are responsible both for the observed L_α–forest and the quasar variability. As remarked earlier, the outer region needs proper modelling, and we intend to return to this in a later paper.

However, there are complicated features for many quasars which are not adequately explained by the simple model exposited in this paper, even with added absorption clouds and strata. For heavier quasars, whose redshift is largely cosmological, the current theory is probably much more appropriate, especially when there are features such as jets which can be observed. We only suggest that our theory fits smaller BHs with high intrinsic redshifts, which are probably much smaller and closer than current theory suggests. Note that very high redshift examples are very dim because of the redshift reduction in energy received and therefore unlikely to be observed.

Finally some wild speculation. We have seen that quasars grow by accretion and lose their intrinsic redshift (as suggested by Arp, but with non-standard physics). If, as Arp suggests, they are ejected from mature galaxies, then there is a natural way to think of them as young galaxies. As they grow and gain mass, they will take on more and more features of active galaxies and perhaps finally develop into mature spiral galaxies. Indeed the quasar–galaxy spectrum has all the appearances of forming the dominant lifeform for the universe.

References

[1] Wikipedia article: *Interstellar medium*, https://en.wikipedia.org/wiki/Interstellar_medium

[2] Wikipedia article: *Wien's displacement law*, https://en.wikipedia.org/wiki/Wien's_displacement_law

[3] **H Arp**, *Sundry articles*, available at http://www.haltonarp.com/articles

[4] **A E Broderick**, **A Loeb**, **R Narayan**, *The event horizon of Sagittarius A**, Astrophys J. 701 (2009) 1357–1366

[5] **R A Flammang**, **K S Thorne**, **A N Zytkow**, Mon Not Roy Astron Soc, 194 (1981) 475–484

[6] **P Galianni**, **E M Burbidge**, **H Arp**, **V Junkkarinen**, **G Burbidge**, **Stefano Zibetti**, *The discovery of a high redshift X-ray emitting QSO very close to the nucleus of NGC 7319*, arXiv:astro-ph/0409215

[7] **J L Greenstein**, **M Schmidt**, *The quasi-stellar sources radio sources 3C48 and 3C273*, Astrophys J. 140 (1964) 1–34

[8] **M R S Hawkins**, *On time dilation in quasar light curves*, Mon Not Roy Astron Soc, 405 (2010) 1940–6

[9] **F Hoyle**, **G Burbidge**, *Anomalous redshifts in the spectra of extragalactic objects*, Astron. Astrophys. 309 (1996) 335–344

[10] **F Hoyle**, **A Fowler**, Nature 213 (1964) 217

[11] **C Leipski**, **K Meisenheimer**, *The dust emission of high-redshift quasars*, J. Phys.: Conf. Ser. 372 (2012) 012037

[12] **M Lopez-Corredoira**, **C M Gutierrez**, *Two emission line objects with $z > 0.2$ in the optical filament apparently connecting the Seyfert galaxy NGC 7603 to its companion*, arXiv:astro-ph/0203466v2

[13] **M Lopez-Corredoira**, **C M Gutierrez**, *Research on candidates for non-cosmological redshifts*, arXiv:astro-ph/0509630v2

[14] **D M Meier**, *Black hole astrophysics: the engine paradigm*, Springer (2009)

[15] **R S MacKay**, **C Rourke**, *Natural flat observer fields in spherically-symmetric space-times*, J. Phys. A: Math. Theor. 48 (2015) 225204, available at http://msp.warwick.ac.uk/~cpr/paradigm/escape-Jan2015.pdf

[16] **R Narayan**, **J E McClintock** *Advection-Dominated Accretion and the Black Hole Event Horizon*, arXiv:0803.0322

[17] **M D'Onofrio**, **J W Sulentic**, **Paola Marziani**, Editors, *Fifty Years of Quasars*, Astrophysics and Space Science Library 386, Springer (2012)

[18] **C Rourke**, *Sciama's principle and the dynamics of galaxies, II: The rotation curve*, submitted for publication, available at http://msp.warwick.ac.uk/~cpr/paradigm/Sciama2.pdf

[19] **C Rourke**, *Sciama's principle and the dynamics of galaxies, III: Spiral structure*, submitted for publication, available at http://msp.warwick.ac.uk/~cpr/paradigm/Sciama3.pdf

[20] **C Rourke**, *Sciama's principle and the dynamics of galaxies, V: Cosmology*, submitted for publication, available at http://msp.warwick.ac.uk/~cpr/paradigm/Sciama4.pdf

[21] **C Rourke**, *Intrinsic redshift in quasars*, available at http://msp.warwick.ac.uk/~cpr/paradigm/hawkins-time-dilation.pdf

[22] **C Rourke**, *Angular momentum, inertial drag and tangential velocity in a rotating dynamical system* http://msp.warwick.ac.uk/~cpr/paradigm/talk.pdf

[23] **A Stockton**, *The nature of QSO redshifts*, Astrophys J. 223 (1978) 747–757

[24] **S Tang**, **S N Zhang**, *Evidence against non-cosmological redshifts of QSOs in SDSS data*, arXiv:0807.2641v2

[25] **D E Vandem Berk**, etal, *Composite quasar spectra from the Sloan digital sky survey*, Astronomical J. 122 (2001) 549–564

[26] **E L Wright**, *Lyman Alpha Forest*, web site at http://www.astro.ucla.edu/~wright/Lyman-alpha-forest.html

Mathematics Institute, University of Warwick, Coventry CV4 7AL, UK

cpr@msp.warwick.ac.uk, R.Toala-Enriquez@warwick.ac.uk, R.S.MacKay@warwick.ac.uk

http://msp.warwick.ac.uk/~cpr, http://www.warwick.ac.uk/~mackay/